Reaction CH 3 + CH 3 → C 2 H 6 Studied over the 292−714 K Temperature and 1−100 bar Pressure Ranges

ARTICLE *in* THE JOURNAL OF PHYSICAL CHEMISTRY A · MAY 2015

Impact Factor: 2.69 · DOI: 10.1021/acs.jpca.5b01276 · Source: PubMed

4 AUTHORS, INCLUDING:

Chao Yan
New Jersey Institute of Technology
3 PUBLICATIONS **1** CITATION

SEE PROFILE

Evgeni Chesnokov
Institute Chemical Kinetics and Combustion
67 PUBLICATIONS **201** CITATIONS

SEE PROFILE

Lev N Krasnoperov
New Jersey Institute of Technology
161 PUBLICATIONS **1,295** CITATIONS

SEE PROFILE

THE JOURNAL OF PHYSICAL CHEMISTRY A

Article

pubs.acs.org/JPCA

Reaction $CH_3 + CH_3 \rightarrow C_2H_6$ Studied over the 292−714 K Temperature and 1−100 bar Pressure Ranges

Manuvesh Sangwan,[†] Chao Yan,[†] Evgeni N. Chesnokov,[‡] and Lev N. Krasnoperov*,[†]

[†]Department of Chemistry and Environmental Science, New Jersey Institute of Technology, University Heights, Newark, New Jersey 07102, United States

[‡]Institute of Chemical Kinetics and Combustion, Novosibirsk 630090, Russia

Supporting Information

ABSTRACT: Reaction of recombination of methyl radicals, $CH_3 + CH_3 \rightarrow C_2H_6$ (1) was studied using pulsed laser photolysis coupled to transient UV−vis absorption spectroscopy over the 292−714 K temperature and 1−100 bar pressure ranges (bath gas He), very close to the high-pressure limit. Methyl radicals were produced by photolysis of acetone at 193.3 nm or in the reaction of electronically excited oxygen atoms $O(^1D)$, produced in the photolysis of N_2O at 193.3 nm, with CH_4, and subsequent reaction of OH with CH_4. Temporal profiles of CH_3 were recorded via absorption at 216.36 and 216.56 nm using a xenon arc lamp and a spectrograph. The absolute intensity of the photolysis light inside the reactor was determined by an accurate *in situ* actinometry based on the ozone formation in photolysis of $N_2O/O_2/N_2$ mixtures. The rate constant of reaction 1 in the high-pressure limit has a negative temperature dependence: $k_{1,inf} = (5.66 \pm 0.43) \times 10^{-11}(T/298\ K)^{-0.37}$ cm^3 $molecule^{-1}$ s^{-1} (292−714 K).

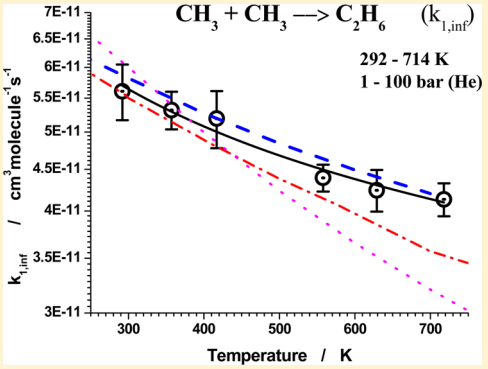

INTRODUCTION

Self-reaction of methyl radicals (channels 1a and 1b) is important in hydrocarbon pyrolysis and combustion mechanisms:[1−11]

$$CH_3 + CH_3 \rightarrow C_2H_6 \quad (1a)$$

$$\rightarrow C_2H_5 + H \quad (1b)$$

Channel 1a is a chain termination step, whereas channel 1b is one of the chain propagation steps. Both the branching ratio and the rate of reaction 1 have an impact on the self-ignition threshold, flame propagation speed, and other parameters of combustion. The reaction is responsible for production of C2 hydrocarbons in methane combustion. Reaction 1 is important for fundamental chemical kinetics and is considered a benchmark reaction for testing and improving theories of radical−radical reactions as a simplest reaction of recombination of hydrocarbon free radicals.[1] Precise knowledge of the kinetic parameters of reaction 1 is nessassary in laboratory studies of other reactions involving methyl radicals.[12,13] In relative kinetic studies involving methyl radicals, reaction 1 was frequently used as a reference reaction.

The disproportionation channel 1b has an appreciable activation energy (56.5 kJ mol^{-1} [8]) and becomes important at temperatures significantly exceeding the highest temperature of the current study (k_{1b}(714 K) = 3.6×10^{-15} cm^3 $molecule^{-1}$ s^{-1} [8]); therefore, it can be completely neglected over the temperature range of this study.

Due to the importance of reaction 1 to the field, it was extensively studied both experimentally and theoretically. There are numerous publications associated with the kinetics of reaction 1, for a detailed bibliography the readers are referred to the NIST database[8] as well as to the bibliography in several recent publications and reviews.[2,14] Even though reaction 1 has been studied across a wide temperature range, only a few studies were conducted at pressures high enough for more reliable determination of the rate constant in the high-pressure limit. Hippler et al.[15] studied reaction 1 over the pressure range 1−210 bar at ambient temperature in two bath gases, argon and nitrogen, using laser photolysis coupled to transient UV absorption. The high-pressure limit was reached at ca. 10 bar of Ar (within the experimental uncertainty); the determined recombination rate constant in the high-pressure limit is $k_{1a,\infty} = 5.8 \times 10^{-11}$ cm^3 $molecule^{-1}$ s^{-1}. A drop of the measured recombination rate constant at higher pressures (ca. 12% in Ar and ca. 3 times in N_2 at 210 bar) was attributed to the onset of diffusion control.

The main motivation of the current work was extension of the study to cover a temperature range from ambient to

Special Issue: 100 Years of Combustion Kinetics at Argonne: A Festschrift for Lawrence B. Harding, Joe V. Michael, and Albert F. Wagner

Received: February 9, 2015
Revised: May 8, 2015

DOI: 10.1021/acs.jpca.5b01276
J. Phys. Chem. A XXXX, XXX, XXX−XXX

elevated temperatures (293−714 K) in the conditions of only minor deviations from the high-pressure limit.

EXPERIMENTAL SECTION

Experimental Setup. The experimental setup is described in details elsewhere;[16−19] therefore, only a brief description critical for the current experiments is given here. The approach is based on the excimer laser photolysis coupled to UV−vis transient absorption spectroscopy and to a high-pressure flow system. Helium was used as a bath gas in all experiments. The measurements were performed over the 1−100 bar pressure and 19−441 °C (292−714 K) temperature ranges. A detailed description of the heatable high-pressure flow reactor employed in this study is given in our previous works.[16−19] Two UV-grade silica or MgF_2 windows (12.7 diameter, 9.5 mm thick) were sealed at the ends of the reactor at ambient temperature outside the high-temperature zone using Viton O-rings. The reagents were supplied through a 3.175 mm o.d. ($^1/_8$ in.) stainless steel tube passed seven times (total length 140 cm) through the aluminum block of the reactor heater for preheating. Such an arrangement ensured complete preheating of the reactant mixture to the reactor temperature without using additional ovens and temperature controllers. The preheated reactant mixture entered the reactor tube in the center and left through the two outlets located on two sides 5 cm away from the center but within the uniform temperature zone. Additional flows of the bath gas (He) entered the reactor near the windows to flush gas from the windows toward the outlets. Two additional thick (9.5 mm) fused silica or MgF_2 windows, separated by a stainless steel insert, were placed without sealing inside the reactor near the reactor outlets. This "four windows" configuration (two outside windows sealed and kept at room temperature and two inside windows, not sealed, limiting the reactive mixture within the homogeneous temperature zone) prevented penetration of the reactants out of the observation zone, provided precise definition of the observation zone within the uniform temperature region, and allowed avoiding of windows sealing at elevated temperatures. The length of the inset determined the optical path in the zone of reactants of 10.13 cm. To achieve uniform concentration profiles across the reactor cross-section, the laser beam was formed using a spherical lens (f = +30 cm, the distance from the reactor center 82 cm) and a cylindrical lens (f = +30 cm, the distance from the reactor center 35 cm). The beam profile was measured by scanning with a small hole diaphragm (ca. 0.5 mm) combined with an energy meter. The beam uniformity across the reactor cross-section was ±7.3% from the mean value. More details of the experimental arrangements and the signal accumulation are described elsewhere.[16−21] The gas flow rates were controlled by high-pressure mass flow controllers (Brooks, model 5850). The total flow rates of the reactant mixtures with helium were in the range 340−4600 sccm (standard cubic centimeters per minute). Additional flush flows to the cold reactor windows were in the range 270−600 sccm.

The axial temperature profiles were measured in 1 cm steps along the reactor length for each set of the experimental conditions (the temperature set points, total flows, and pressures) used in the kinetic measurements. The temperature profiles were uniform within ±5 K in the reactants zone. The average temperature in the reactant zone was taken as the reactor temperature.

Acetone−water mixtures were degassed using three freeze−pump−thaw cycles before loading in the stainless steel syringe. The mole fraction of acetone in water was varied from 0.02 to 0.04. Acetone−water mixtures were injected into the evaporator of the high-pressure flow system using a precision syringe pump (Harvard Apparatus, Model PHD 4400) through a capillary tube. The temperature of the evaporator was kept at 90 °C, it was observed that this approach produced steady and stable flows of acetone−water gas mixtures over the pressure range 1−100 bar. The flow rate of acetone−water mixtures was varied in the range of 0.5−10 μL/min depending upon the reactor pressure and temperature. The concentrations of the precursors used were (0.1−1.0) × 10^{17} molecules cm^{-3} for N_2O, (0.87−6.76) × 10^{15} for CH_3COCH_3, and (1.4−7.0) × 10^{17} for H_2O. The laser photon fluence inside the reactor was varied in the range (2.4−15) × 10^{15} photons cm^{-2} $pulse^{-1}$. The initial concentrations of methyl radicals were in the range (5−46) × 10^{13} molecules cm^{-3}. The measurements were performed over the 1−100 bar (He) pressure and 292−714 K temperature ranges. The concentrations of the radicals precursors were monitored downstream from the reactor by an online quadrupole mass-spectrometer (Finnigan 4021) at m/z = 43, 44 for N_2O and m/z = 58 for acetone, relative to the signal of argon added to the mixture (0.001% of argon, m/z = 40). No noticeable depletion of the radical precursors (acetone and nitrous oxide) was observed at and below above 714 K. Separately these compounds were stable up to the highest temperature of the reactor of 834 K. The repetition rate of the laser was set to ensure complete replacement of the gas mixture in the reactor between the pulses (0.1−1 Hz depending upon the reactor pressure).

In Situ Actinometry. One of the most important requirements in studying the radical−radical reactions is reliable determination of the absolute concentrations of free radicals. To determine radical concentration accurately, it is necessary to know the photon fluence inside the reactor. In this work, the absolute concentrations of OH and CH_3 radicals were determined on the basis of the photon fluence inside the reactor, the absorption cross sections of N_2O and acetone at 193.3 nm, and the efficiency of conversion of $O(^1D)$ atoms produced in the photolysis of N_2O/CH_4 mixtures to CH_3 radicals. The efficiency was typically ca. 0.79 × 2 and was accurately evaluated using a reaction mechanism (complete detailed mechanism is given in Table 2 of ref 13). The absorption cross-section of N_2O is accurately known at 298 and 1 bar. At other conditions, the cross sections of N_2O were measured in previous work.[19] The absorption cross section of acetone was determined in ref 13 (Supporting Information for ref 13). The major source of errors is in the determination of the laser light intensity inside the reactor. Outside laser energy meters require calibrations, in addition to having windows transmittance drift due to film deposition caused by contaminations introduces additional errors. In this work, we used an *in situ* laser light actinometry based on the stable molecule formation with very well characterized cross-section at a monitoring wavelength. Specifically, ozone formation, monitored at 253.7 nm, in the photolysis of $N_2O/O_2/N_2$ mixtures at 1 bar and 298 K, was used. Details of this technique can be found in our previous work.[19]

Usually, two such determinations were performed, before and after a series of measurements. Simultaneously, the readouts of the pyroelectric detector measuring laser pulse energy after the reactor were recorded.[19] The readouts of the pyroelectric detector in the kinetic measurements were used

DOI: 10.1021/acs.jpca.5b01276
J. Phys. Chem. A XXXX, XXX, XXX−XXX

then to introduce proper corrections for the drift of the laser energy during a series of experiments.

Reagents. In the initial experiments UHP grade helium (99.9995%) from Airgas passed through an in-line oxygen trap (R&D Separations, Model OT2-SS, manufacturer stated oxygen content reduction to 15 ppb) was used. Later, it was replaced with BIP Helium from Airgas with 99.9999% purity with reduced oxygen content (<10 ppb). Pure nitrous oxide was obtained from Scott Specialty Gases (99.9995%). In the high-pressure experiments, certified mixture of N_2O in He (mole fraction of 0.025, the accuracy ±2%) obtained from AirGas, was used. Purified water (Milli-Q) with TOC less than 5 ppb) was degassed by using three freeze−pump−thaw cycles and used as a solvent for acetone/water solutions supplied by the syringe pump (Harvard Apparatus PHD4400). Acetone used in the acetone−water mixtures was purchased from Fisher Scientific (99.7%). Methane UHP 300, 4.0 grade, was purchased from AirGas.

CH_3 Radicals Generation and Monitoring. CH_3 radicals were generated by excimer laser pulse photolysis either of acetone

$$(CH_3)_2CO + h\nu(193\,nm) \rightarrow 2CH_3 + CO \quad (2a)$$

$$\rightarrow CH_2COCH_3 + H \quad (2b)$$

$$\rightarrow CH_4 + CH_2CO \quad (2c)$$

or of N_2O in the presence of methane at 193.3 nm (ArF excimer laser):

$$N_2O + h\nu(193\,nm) \rightarrow O(^1D) + N_2 \quad (3a)$$

$$\rightarrow N(^4S) + NO(^2\Pi) \quad (3b)$$

$$O(^1D) + CH_4 \rightarrow OH + CH_3 \quad (4)$$

$$OH + CH_4 \rightarrow H_2O + CH_3 \quad (5)$$

In the photolysis of acetone at 193.3 nm, in addition to the major channel 2a resulting in two methyl radicals, there are two other possible channels, reactions 2b and 2c. The quantum yields of channels 2a−c at 193 nm were measured by Lightfoot et al.[22] as $\phi_{2a} = 0.95$, $\phi_{2b} = 0.03$, and $\phi_{2c} = 0.02$ at 300 K with a negligible temperature dependence (over the 300−600 K temperature range).

The quantum yield of the major channel 3a is unity within 1%; the minor channel 3b is less than 0.8%.[23] A fraction of $O(^1D)$ formed in photolysis of N_2O reacts with N_2O:

$$O(^1D) + N_2O \rightarrow NO + NO \quad (6a)$$

$$\rightarrow O_2 + N_2 \quad (6b)$$

$$\rightarrow O(^3P) + N_2O \quad (6c)$$

It was indicated that methyl radical might be further photolysied by the laser light during the laser pulse:[24]

$$CH_3 + h\nu(193.3\,nm) \rightarrow CH_2 + H \quad (7)$$

The estimated fraction of methyl radicals at the fluence of 35 mJ cm^{-3} is less than 2%.[24] The fraction of methyl radical photolyzed by the same laser pulse (α) can be estimated using eq E1:

$$\alpha = \phi\sigma_{193}(CH_3)/2 \quad (E1)$$

where ϕ is the laser fluence (in photon cm^{-2}) and $\sigma_{193}(CH_3)$ is the absorption cross-section of CH_3 radicals at the laser wavelength 193.3 nm. Expression E1 is valid irrespective of the laser pulse shape and duration, provided that the pulse is much shorter than the decay time of CH_3 radicals, the absorption cross-section does not change during the pulse (e.g., due to the vibrational relaxation of CH_3 radical), and the fraction α is small. According to the spectrum simulations,[14] the absorption cross-section of CH_3 at 193.3 nm increases with the internal energy of methyl radicals. At 1500 K the cross-section at 193.3 nm is smaller than 1×10^{-18} cm^2 $molecule^{-1}$.[14] At the fluence of 10 mJ cm^{-2} (ca. 10^{16} photons cm^{-2}), eq E1 results in $\alpha <$ 0.5%. This is in accord with the estimate made in ref 24. Therefore, for the laser fluences (<10 mJ cm^{-2}) used in this study the secondary photolysis of methyl radicals during the same laser pulse (7) could be neglected.

The decay of methyl radicals was monitored by absorption at 216.36 and 216.56 nm (1200 groove/mm grating, 300 mm focal distance, both slits 0.25 mm, triangle slit function, FWHM = 0.64 nm) using a 75 W (Oriel) short arc xenon lamp combined with an imaging spectrometer (Acton 300i).

A 75 W xenon short arc lamp was used as a light source. In some experiments the lamp intensity was increased (ca. 100 times at 216 nm) by current boosting to 50 A using Photon Technology International MCP2010 pulser. The imaging spectrograph (Acton 300i) is equipped with three diffraction gratings (1200, and two 150 groove/mm), a PMT (Hamamatsu R106) with a preamplifier (EMI) and a gated intensified CCD (ICCD) camera (ICCD Max, Roper Scientific). The residual light from the excimer laser pulse is blocked using a liquid filter (4.3×10^{-2} M solution NaCl in water, 1 cm). The liquid filter provides virtually complete absorption of 193 nm light. A photomultiplier tube (Hamamatsu R106) mounted on the exit slit operates on a reduced number of dynodes (6) with a large high-voltage divider current (maximum 2.7 mA), which ensures good linearity and lower noise at high photon fluxes. The typical anode current is 10−20 μA. The PMT signal is preamplified (EMI preamplifier), digitized, and stored using a digital storage oscilloscope (LeCroy 9310A, Dual channel, 400 MHz, 100 Msamples/s, 50 Kpts/ch). The time resolution is determined by the preamplifier setting and can be 0.03, 0.3, 3, or 30 μs. Typically, a 0.3 μs time constant was used (the measured actual rise time $t_{0.1-0.9}$ is 0.46 μs). The traces are accumulated (500−5000 pulses) and transferred to a PC for processing. The ICCD camera installed on the second outlet of the spectrograph is used to record absorption spectra of transient as well as stable species.

In all measurements, monitoring light intensity traces were accumulated also in the absence of the precursor molecules (i.e., acetone or N_2O). Subsequently, these traces were subtracted from the traces acquired in the presence of the precursors. This was done to exclude the effect of the monitoring light intensity change upon the exposure of the multilayer mirrors to the laser pulse (hereafter dubbed as "zero shift"). Such a change is caused by the partial release of water from the porous layers of multilayer coating as well as a small temperature change of the mirror coatings. These factors lead to small change of the indexes of refraction of the coating layers materials and, subsequently, to the modulation of the mirrors reflectivity. The "zero shift" could be negative and positive depending on the spectral separation of the monitoring wavelength from the wavelength of the maximum reflectivity of the mirrors and was observed in all experiments where the

DOI: 10.1021/acs.jpca.5b01276
J. Phys. Chem. A XXXX, XXX, XXX−XXX

same approach of merging of the photolysis and monitoring beams was used.[13,25−29] In this study, the typical scale of the "zero shift" was ca. 4×10^{-4}. In addition, subtraction of the "zero shift" trace did eliminate a minute distortion after the large spike caused by the reactor windows luminescence (of a similar scale, $(2-4) \times 10^{-4}$).

RESULTS

Absorption spectrum of CH_3 radicals is temperature and pressure dependent. Detailed analysis of the absorption spectrum for the $\tilde{B}^2A_1' \leftarrow \tilde{X}^2A_2''$ in the vicinity of 216 nm as well as a review of previous experimental measurements and modeling is given in a recent paper of Blitz et al.[14] The individual rotational lines are strongly broadened by predissociation; therefore, the spectrum has no rotational structure. The electronic transition $\tilde{B}^2A_1' \leftarrow \tilde{X}^2A_2''$ as well as the associated absorption spectrum of methyl radical have been extensively studied experimentally and theoretically.[14,30−33]

To understand the changes in the apparent cross-section of methyl radical taken with a finite spectral slit widths, we recorded the absorption band at 216 nm with the highest resolution achievable in the current experimental setup (1200 groove/mm, focal distance 300 mm, slit width 10 μm, camera pixel size of 30 um) using current boosted Xe arc lamp and a gated ICCD camera. A 75 W Xe short arc lamp was boosted up to 50 A for 7 ms. The spectra were taken 0.9 μs after the laser pulse (delayed by ca. 6 ms after the beginning of the boosting pulse) with the time gate of 2 μs. The results are shown in Figure 1 for the extremal combinations of temperature and pressure. Increasing pressure to 100 bar leads to a substantial broadening of the spectrum accompanied by a blue shift of the maximum (ca. 0.22 nm at 100 bar).[15] The main peak at 216.36 nm is mainly due to the vibrational ground to vibrational ground transition between the ground and excited electronic states, $\tilde{B}^2A_1'(0,0,0,0) \leftarrow \tilde{X}^2A_2''(0,0,0,0)$ (the Franck−Condon factor of 0.764).[14,31] The other transitions with appreciable Franck−Condon factors originating from the ground vibrational state of the X-state are the transition to the $v_1' = 1$ in the excited state, $\tilde{B}^2A_1'(1,0,0,0) \leftarrow \tilde{X}^2A_2''(0,0,0,0)$ (Franck−Condon factor of 0.162) and the transition to the overtone $v_2 = 2$ in the excited B-state (the Franck−Condon factor = 0.048).[31] These transitions are peaked at ca. 208 nm and are broader than the main peak at 216 nm. There is a "hot" transition at ca. 212.7 nm, the intensity of this peak increases with temperature (Figure 1). The peak was identified as hot $\tilde{B}^2A_1'(0,1,0,0) \leftarrow \tilde{X}^2A_2''(0,1,0,0)$ transition.[34] The "shoulder" on the blue side of the main peak observed at low temperatures is due to the contributions of these three transitions.

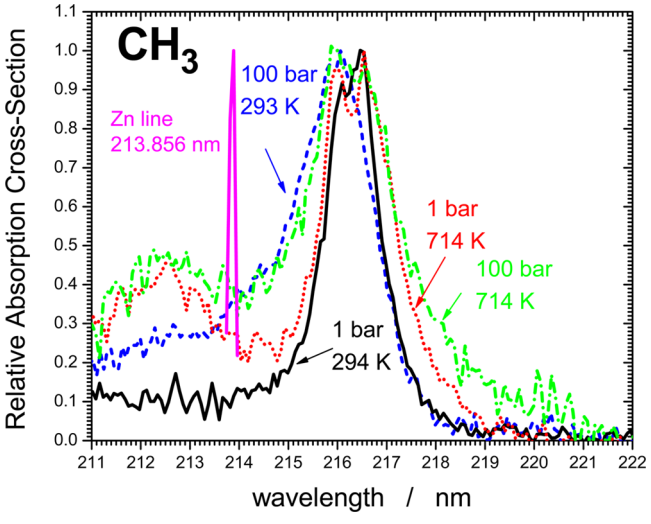

Figure 1. Absorption spectra of the CH_3 radical near 216 nm at different experimental conditions. Slit 10 um, pixel size 30 μm, 1200 groove/mm grating, spectral resolution 0.15 nm (FWHM). Solid line: 294 K, 1 bar. Dotted line: 714 K, 1 bar. Dashed line: 293 K, 100 bar. Dash-dotted line: 714 K, 100 bar. Narrow feature: Zn resonance emission line (213.856 nm). The spectra were obtained using a gated ICCD camera (ICCD Max, Princeton Instruments), the delay after the laser pulse 0.9 μs, gate 2 μs. Light source: current boosted 75 W Xe arc lamp (current pulse 50 A).

In the kinetic measurements, wider slits (0.25 mm) were employed. This corresponds to the triangular spectral slit function with the FWHM = 0.64 nm. Convolution of the spectra obtained with 10 μm slit and ICCD detection with the triangular FWHM = 0.64 nm slit function shows almost no impact on the widths of the spectra with some reduction of the maximum apparent cross-section. It is most pronounced at 1 bar and ambient temperature, where the maximum cross-section of the convoluted spectrum drops by 12 ± 3%. The wavelength of the maximum of the apparent cross-section shifts with temperature and pressure. In the current study, two central wavelengths were used: 216.36 nm, which corresponds to the small hole in the main peak and the maximum apparent cross-section at ambient temperature and pressure when taken with the resolution of 0.64 nm, and 216.56 nm, which corresponds to the maximum of the high-resolution spectrum. This wavelength (216.56 nm) was used in our previous work on the kinetics of the CH_3 + OH reaction; therefore, the cross sections reported here are slightly different (larger) from the cross sections reported previously (Supporting Information for ref 19).

In the calculations of the reactants concentrations small deviations from the ideal gas behavior were taken into account. The deviations from ideal gas equation of state are tabulated.[35] The compression factor for He is 1.0471 at 300 K and 1 bar. The deviations decrease at low pressures and higher temperatures.

Apparent absorption cross sections of methyl radicals were measured with the triangular spectral slit function with FWHM = 0.64 nm using the two central wavelengths. The apparent cross sections obtained at 216.56 nm were reported previously (Supporting Information for ref 13). This is the wavelength that corresponds to the maximum of the Q+P peak in the double-peaked absorption spectrum of methyl radical at room temperature. Although this wavelength provides the maximum absorption cross-section at ambient temperature and pressure for narrow line light sources, for the line width of 0.64 nm employed in this work the maximum apparent cross-section is for the central wavelength that corresponds to the small hole in the spectrum between the R and Q+P peaks, 216.36 nm. The apparent cross sections at these wavelengths measured at different temperatures and pressures are summarized in Tables 1 and 2.

It should be stressed that due to the pressure induced blue shift of the absorption line neither central wavelength 216.36 nor 216.56 nm provide the maximum absorbance at the conditions different from 1 bar and 298 K, especially at high pressures (Figure 1). The cross sections measured at p = 1 bar are in good agreement with the measurements of Macpherson et al.[30] Current measurements are ca. 6% lower; however, the

DOI: 10.1021/acs.jpca.5b01276
J. Phys. Chem. A XXXX, XXX, XXX−XXX

Table 1. Product of the Apparent Absorption Cross-Section of Methyl Radical and Half of the Quantum Yield of Methyl Radicals in Photolysis of Acetone at 193.3 nm ($\sigma_{CH_3} \times (\phi_{CH_3}/2)/10^{-17}$ cm^2 molecule^{-1}) at Different Temperatures and Pressures[a]

T/K	1 bar	3 bar	10 bar	30 bar	100 bar
298	3.86	3.23	3.15	3.27	2.15
355	3.51	3.30	3.22	3.04	2.24
414	3.22	2.93	2.97	3.00	2.23
555	2.55	2.45	2.01	2.43	1.85
626	2.33	2.15	2.08	2.10	1.88
714	2.34	1.90	1.57	1.99	1.47

[a]Both slits 0.25 mm, grating 1200 groove/mm, 300 mm focal distance of the spectrograph (triangular slit function with FWHM = 0.64 nm). Central wavelength 216.36 nm. The errors are ca. ±4% at 1 bar and ca. ±7% at 100 bar.

Table 2. Product of the Apparent Absorption Cross-Section of Methyl Radical and Half of the Quantum Yield of Methyl Radicals in Photolysis of Acetone at 193.3 nm ($\sigma_{CH_3} \times (\phi_{CH_3}/2)/10^{-17}$ cm^2 molecule^{-1}) at Different Temperatures and Pressures[a]

T/K	1 bar	3 bar	10 bar	30 bar	100 bar
298	3.55	3.06	3.36	2.34	1.27
355	3.44	2.86		2.15	
414	2.80	2.75	2.81	2.18	1.33
497		2.53		1.87	
555	2.39	2.36	2.42	1.76	1.40
626	2.17	2.09	2.10	1.36	1.18
666	2.01	2.14	2.10	1.35	
714	1.91	1.91	1.77	1.34	1.10

[a]Both slits 0.25 mm, grating 1200 groove/mm, 300 mm focal distance of the spectrograph (triangular slit function with FWHM = 0.64 nm). Central wavelength 216.56 nm. The errors are ca. ±4% at 1 bar and ca. ±7% at 100 bar.

measurements of Macpherson et al. were made at lower pressures (<0.53 bar) and with slightly better resolution (0.6 nm).

Sample temporal profiles of methyl radical absorption at 216.36 nm in photolysis of acetone are shown in Figure 2. The measurements were made on the submillisecond time scale. In the absence of water, recombination of methyl radicals (reaction 1a) would be the only major elementary reaction responsible for the decay of methyl radicals. In such a case, second-order kinetics is described by

$$\mathrm{Abs}(t) = \mathrm{Abs}_0/(1 + 2\,B\,\mathrm{Abs}_0\,t) \quad \text{(E2)}$$

where Abs(t) is the absorbance (base e), defined via the monitoring light intensity $I(t)$ and the light intensity before the laser pulse, I_0:

$$\mathrm{Abs}(t) = \ln(I_0/I(t)) \quad \text{(E3)}$$

Abs_0 is the absorbance of the monitoring light (216.36 nm) right after the laser pulse, and parameter B is the ratio of the recombination rate constant k_1, the apparent absorption cross-section of methyl radical at the monitoring wavelength, 216.36 nm, and the cell length L:

$$B = k_1/(\sigma_{CH3}L) \quad \text{(E4)}$$

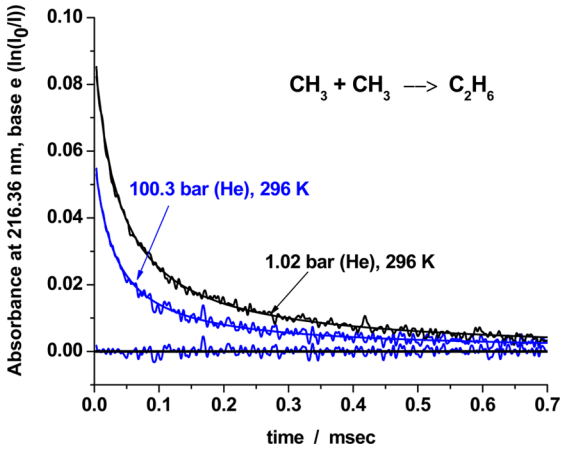

Figure 2. Sample temporal profiles of CH_3 decay. Temperature = 296 K, pressure = 1.02 bar (upper curve) and 100.3 bar (lower curve), bath gas He. Solid lines: fits by the reaction mechanism (see text). The residual is shown for the 100.3 bar curve. Conditions: $[(CH_3)_2CO]$ = 3.92×10^{15} and 1.63×10^{15} molecules cm^{-3}, laser fluences 8.64×10^{15} and 9.99×10^{15} photon cm^{-2} for the profiles at 1.02 and 100.3 bar, respectively.

Expression 1 is valid only when attenuation of the laser radiation resulting from the precursor's absorption is relatively small (<5−10%). In the case of strong absorption of the laser light, exact expression accounting for the nonuniform axial initial concentration of methyl radicals was used:

$$\mathrm{Abs}(t) = (2\,B\,\ln(G)\,t)^{-1}\ln\frac{(1 + 2\,\mathrm{Abs}_0\,G\,\ln(G)\,B\,t/(G-1))}{(1 + 2\,\mathrm{Abs}_0\,\ln(G)\,B\,t/(G-1))} \quad \text{(E5)}$$

where G is the parameter characterizing the attenuation of the laser light:

$$G = I_{laser}(x{=}0)/I_{laser}(x{=}L) \quad \text{(E6)}$$

It should be noted that numerical comparison of eqs 3 and 4 for the initial absorbance of 0.3 results in a somewhat counterintuitive result. Using eq 3 to fit the profiles simulated using eq 4 results only in 0.6% error in the signal amplitude and in 0.8% in the parameter B, when half of the laser light intensity is absorbed (G = 2). Even at much higher attenuation (G = 5, 20% of laser light is passing through) the errors are still reasonable: 4.3% in the signal amplitude and 3.3% in the B parameter.

To work with a convenient and reliable flow rate of the liquid precursor, we used solutions of acetone in water. The presence of water might potentially result in complications due to the photolysis of water molecules:

$$H_2O + h\nu(193.3\,\mathrm{nm}) \rightarrow H + OH \quad (8)$$

Modeling with the detailed mechanism (ref 13 and the Supporting Information for this paper) using numerical solution of the corresponding system of differential equation showed that the impact of the inclusion of water photolysis on the resulting rate constant 1 does not exceed 1.5%.

The majority of the experiments were done using photolysis of acetone as a source of methyl radicals. The experimental conditions and the results of the measurements are summarized in Tables 3 and 4. Additional series of measurements were carried out using photolysis of N_2O/CH_4/He mixtures. These

DOI: 10.1021/acs.jpca.5b01276
J. Phys. Chem. A XXXX, XXX, XXX−XXX

Table 3. Experimental Conditions and Results[a]

p/bar	T/K	no. density/10^{19} molecules cm^{-3}	$[(CH_3)_2CO]/10^{15}$ molecules cm^{-3}	$[CH_3]/10^{14}$ molecules cm^{-3}	$k_1/10^{-11}$ cm^{3}molecule^{-1} s^{-1}
1.01	292	2.50	3.92	2.15	5.81
1.01	354	2.07	3.21	2.02	5.28
1.01	414	1.77	2.74	1.94	5.11
1.01	558	1.31	2.05	1.71	4.27
1.01	626	1.17	1.82	1.52	4.10
1.02	714	1.03	1.43	0.818	4.27
2.90	294	7.13	4.47	1.97	5.04
2.90	354	5.93	3.71	1.76	4.95
2.90	414	5.07	3.17	1.73	4.67
2.90	555	3.78	2.37	1.50	4.27
2.90	626	3.35	2.10	1.37	4.00
2.90	714	2.94	1.84	1.16	3.87
9.77	294	24.0	4.71	2.27	5.52
9.77	357	19.7	3.91	2.05	5.61
9.77	414	17.0	3.34	1.93	5.33
9.77	555	12.7	2.50	1.68	4.42
9.77	626	11.3	2.22	1.56	4.57
9.77	714	9.89	1.94	1.32	4.10
30.32	294	73.6	2.02	2.17	6.06
30.32	354	61.3	1.68	1.85	5.43
30.32	414	52.5	1.44	1.56	5.66
30.32	555	39.3	2.17	2.45	4.62
30.32	626	34.8	1.92	2.29	4.29
30.32	714	30.6	1.69	1.95	4.29
100.3	296	234	1.63	2.45	5.88
100.3	354	197	1.36	1.91	5.34
100.3	414	170	1.41	2.13	4.64
100.3	555	128	1.24	1.85	3.76
100.3	626	113	1.26	1.76	4.32
100.3	714	99.8	1.38	1.83	3.87

[a]Photolysis of acetone at 193.3 nm as a source of CH_3 radicals. Central wavelength 216.36 nm.

results together with the experimental conditions are listed in Table 5.

Selected series of measurements are shown in Figures 3 and 4. Figure 3 illustrates the scatter of the experimental points, the stability of the resulting rate constants with respect to the attenuation of the laser radiation, and the consistency of the results obtained in the photolysis of acetone and N_2O/CH_4 mixtures. The results of the measurements of the cross-section as well as the rate constant of reaction 1 at 714 K and 100 bar in the two photolysis systems at different attenuations of the laser light (expressed as the initial absorbance amplitude of methyl radicals) are shown in Figure 4. Maximum scatter of the experimental data does not exceed ±16%. Both photolysis systems produce consistent results indistinguishable within the experimental scatter.

There are two major factors contributing to the errors in the measurement. First comes from the scatter of the ratio k_1/σ_{CH_3} (which is determined directly from the decay profiles and does not require actinometry). The second is the accuracy of the determination of the photon fluence inside the reactor.

Review of 44 decay profiles recorded at ambient temperature and 1 bar at different initial concentrations of methyl radicals over a period of several years reveals that the major source of errors in this work originates from the scatter of the ratio k_1/σ_{CH_3}. The histogram is shown in Figure 5. The scatter is caused by the reproducibility of the central wavelength (0.05 nm as stated by the manufacturer) as well as the accuracy of the fit limited by the signal-to-noise ratio in the experimental decay profiles. The standard deviation of the scatter is ca. 9%. A conservative estimate on the accuracy of the in situ actinometry used is about 7%, which independently combines to ca. 12% error in the rate constant.

Investigation of the kinetic results reveals two major features. First, there is a systematic drop in the measured apparent rate constant at 100 bar pressure as compared with the measurements at 1 bar. This is shown in Figure 3. Second, no rise of the apparent rate constant was observed within the accuracy of the measurements at 714 K, where some rise due to the pressure falloff could be expected.

Potentially, the drop of the rate constant with pressure could be caused by several factors. It could be due to the quenching of the primary photolysis processes 2a and 3a. Due to the large difference in the complexity of the two precursors, acetone and N_2O, this cause does not seem to be probable. Another possibility would be the onset of the diffusion control. And, finally, closely associated with the diffusion control, cage effects in the photolysis of the precursors as well as reaction 4 might be responsible for the drop of the initial concentrations of methyl radicals in the bulk and, hence, the apparent rate constant.

Diffusion control as well as the cage effect in dense media are well established phenomena.[36−41] In application to reaction 1 the impact of diffusion control was discussed in ref 15. The 15−20% drop at ambient temperature corresponds to the diffusion-controlled rate constant of $k_{diff} = (2.3−3.3) \times 10^{-10}$ cm^3

DOI: 10.1021/acs.jpca.5b01276
J. Phys. Chem. A XXXX, XXX, XXX−XXX

Table 4. Experimental Conditions and Results[a]

p/bar	T/K	no. density/10^{19} molecules cm^{-3}	$[(CH_3)_2CO]/10^{15}$ molecules cm^{-3}	$[CH_3]/10^{14}$ molecules cm^{-3}	$k_1/10^{-11}$ cm^{3}molecule^{-1} s^{-1}
1.01	292	2.50	1.9	1.03	5.89
1.01	354	2.07	0.93	1.02	5.87
1.01	414	1.77	1.85	1.17	4.71
1.01	558	1.31	1.57	1.02	4.62
1.01	626	1.17	1.54	0.887	4.15
1.01	669	1.09	1.35	0.772	4.22
1.01	714	1.02	1.12	0.755	3.83
2.88	293	7.11	4.44	0.873	5.65
2.88	354	5.89	3.73	0.848	4.55
2.88	414	5.03	3.19	0.795	4.61
2.88	497	4.19	2.66	0.709	4.15
2.88	555	3.76	2.38	0.664	3.86
2.88	626	3.33	2.12	0.593	3.18
2.88	669	3.12	1.98	0.563	3.19
2.88	714	2.92	1.85	0.547	3.36
9.84	294	24.1	6.76	2.01	5.67
9.84	414	17.2	4.78	1.82	4.81
9.84	555	12.8	3.58	1.56	4.62
9.84	626	11.4	3.18	1.38	4.36
9.84	669	10.6	2.97	1.31	4.31
9.84	714	9.96	2.78	1.30	4.29
30.51	294	74.1	5.06	1.51	5.78
30.51	354	61.7	4.17	1.56	4.86
30.51	414	52.8	3.58	1.70	4.42
30.51	497	44.1	3.00	1.56	3.49
30.51	555	39.5	2.69	1.47	3.43
30.51	626	35.1	2.39	1.26	3.35
30.51	669	32.8	2.23	1.10	3.50
30.51	714	30.8	2.10	1.04	3.36
100.8	298	234	2.00	1.56	4.60
100.8	414	170	1.47	1.17	4.17
100.8	555	128	0.99	0.64	4.24
100.8	555	128	1.11	0.92	4.43
100.8	626	114	0.994	0.64	3.47
100.8	626	114	1.66	1.17	3.11
100.8	714	100	0.875	0.609	4.20
100.8	714	100	2.19	1.39	4.23

[a]Photolysis of acetone at 193.3 nm as a source of CH_3 radicals. Central wavelength 216.56 nm.

Table 5. Experimental Conditions and Results[a]

p/bar	T/K	no. density/10^{19} molecules cm^{-3}	$[N_2O]/10^{16}$ molecules cm^{-3}	$[CH_4]/10^{19}$ molecules cm^{-3}	$[CH_3]/10^{14}$ molecules cm^{-3}	k_1/σ_{CH_3} 10^6 cm s^{-1}	$k_1/10^{-11}$ cm^{3}molecule^{-1} s^{-1}
100.4	293	237	1.84	5.69	2.53	3.99	5.63
100.4	293	237	3.63	5.67	4.60	4.31	5.26
100.4	294	235	9.16	5.66	0.978	3.64	5.31
100.4	294	235	9.16	5.66	1.07	3.24	4.21
100.4	294	235	3.60	5.63	3.62	3.63	4.76
100.4	294	235	5.50	5.67	0.574	3.41	4.50
100.8	714	99.7	6.86	2.07	3.09	2.95	3.59
100.8	714	99.7	3.46	2.07	1.60	3.31	3.42
100.8	714	99.7	2.77	2.07	1.26	3.85	3.48
100.8	714	99.7	3.47	1.64	1.50	2.68	2.84

[a]Reactions $O(^1D)$ and, subsequently, OH with CH_4 as a source of CH_3 radicals (photolysis of N_2O/CH_4/He mixtures at 193.3 nm). Central wavelength 216.56 nm.

molecule^{-1} s^{-1}. For an isotropic reaction of spherical particles A and B, the diffusion-controlled rate constant is $k_{diff} = 4\pi R_{AB} D_{AB} = 4\pi(R_A + R_B)(D_A + D_B)$. For a self-reaction A + A, like the recombination of methyl radicals, this expression should be divided by 2, resulting in $k_{diff} = 8\pi R_A D_A$. Estimating $D(CH_3-He)$ as $D(CH_4-He) = 0.73 \times 10^{-2}$ cm^2 s^{-1} at 293 K and 100 bar[42] leads to the radius R = 0.015 nm = 0.15 Å. However, recombination of methyl radicals is highly anisotropic, and

DOI: 10.1021/acs.jpca.5b01276
J. Phys. Chem. A XXXX, XXX, XXX−XXX

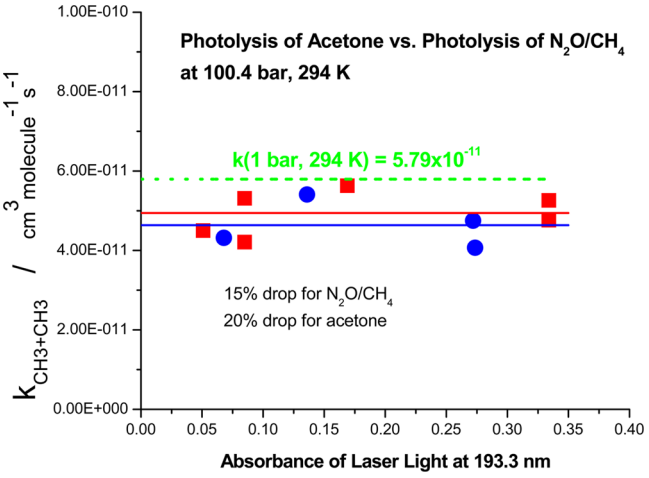

Figure 3. Comparison of the photolysis of acetone and N_2O/CH_4 at 193.3 nm, 100.4 bar, and 294 K. Returned rate constant as a function of the attenuation of laser light. Squares: photolysis of N_2O/CH_4. Circles: photolysis of acetone. Dashed line: results of the measurements at 1 bar, 294 K. Systematic deviation of all experimental points from the results at 1 bar is apparent. The average values are a 15% drop of the rate constant determined using N_2O/CH_4 photolysis and a 20% drop using photolysis of acetone when going from 1 to 100 bar. The difference of the two measurements is within the precision; the difference with the measurements at 1 bar is outside the error limits.

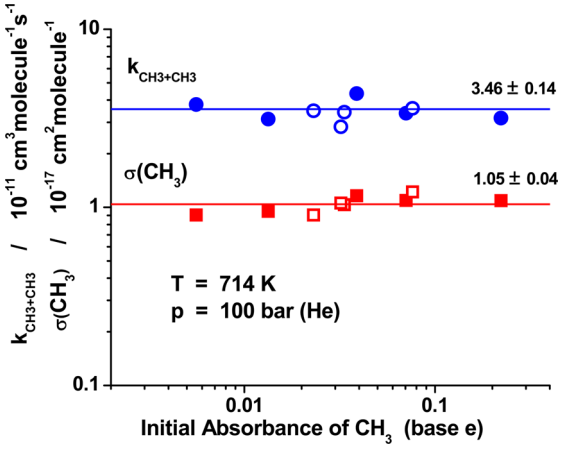

Figure 4. Comparison of the photolysis of acetone and N_2O/CH_4 at 193.3 nm, 100.4 bar, and 714 K. Returned rate constants and cross sections as a function of the initial absorbance of methyl radicals. Empty symbols: photolysis of N_2O/CH_4. Filled symbols: photolysis of acetone. Squares: cross-section of CH_3 radical at 216.36. Circles: rate constant of reaction 1.

using the expression $4\pi R_{AB}D_{AB}$ is not justified. In this expression, $4\pi R_{AB}^2$ is the area of the sphere where the diffusion flux is calculated, and the factor $1/R_{AB}$ is coming from the gradient of the concentration at the surface of the sphere. In the same spirit, setting the characteristic size d for the "active" spot on the reactive surface, and the same characteristic length for the concentration gradient evaluation, taking into account two "reactive spots" of CH_3 radical, leads to an estimate

$$k_{diff} \approx (1/2)2dD_A \quad \text{(E7)}$$

Equation E7 leads to a more realistic estimate for the characteristic "reactive spot" size of ca. 0.38 nm = 3.8 Å. This estimate shows that potentially diffusion control might play

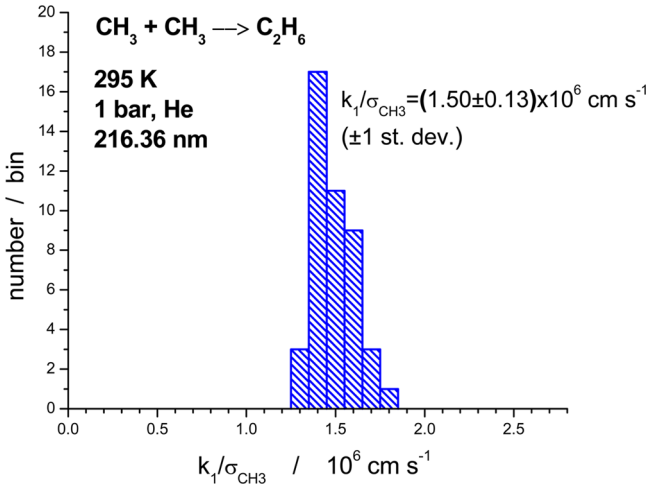

Figure 5. Histogram of the distribution of the rate constant−cross section ratio (k_1/σ_{CH_3}) obtained at the central wavelength of the monitoring light of 216.36 nm at 1 bar (He) and 295 ± 3 K. Both slits 0.25 mm, grating 1200 groove/mm, 300 mm focal distance of the spectrograph (triangular slit function with FWHM = 0.64 nm).

some role at 100 bar. The cage effect is closely related to the diffusion control; similar estimates are applicable. Comparable effects were observed in recombination of CCl_3 radicals at comparable pressures[43] and assigned to the diffusion control. Therefore, the observed drop of the recombination rate of methyl radicals could be tentatively assigned to onset of the diffusion control; however, further investigation of the subject is necessary.

The observed drop of the recombination rate constant at 100 bar is ca. 15−20%. Therefore, the expected decrease of the rate constant due to the onset of the diffusion control at 30 bar (the highest pressure included in the rate constant averaging) is ca. 5−7%. The drop in the rate constant averaged over 1, 3, 10, and 30 bar is expected not to exceed ca. 2%.

Decrease of the rate constant of methyl radicals recombination was observed previously by Hippler et al.[15] at ambient temperature in argon and nitrogen bath gases. The observed drop of the rate constant in Ar was ca. 4% at 100 bar and ca. 12% at 210 bar, smaller than that observed in He in this work (ca. 15−20% at 100 bar). A much larger drop was observed when nitrogen was used as the bath gas, ca. factor of 2 at 100 bar and ca. factor of 3 at 200 bar.[15] Neither the scale of the effects nor the relative order for different bath gases correspond to the diffusion control limited by translational diffusion of the reactants. In view of highly anisotropic interaction of methyl radicals, orientation relaxation rather than translational diffusion might be responsible for the observed decrease in the recombination rate.

The second feature is the absence within the experimental accuracy of any rise of the rate constant with pressure at 714 K over the range 1−100 bar. Estimates based on the recommended low-pressure limit rate constant k_0(714 K) = 5.28×10^{-28} cm^6 molecule^{-2} s^{-1} [44] and the high-pressure rate constant of 3.14×10^{-11} cm^3 molecule^{-1} s^{-1} [50] lead at 1 bar and 714 K to the ratio $x = k_0[M]/k_{inf} = 171$. Both the extrapolations based on the standard Troe formalism[45] and the recent approach of Zhang and Law[46] result in the prediction of ca. 25% drop of the rate constant at 1 bar compared with the 100 bar value. Accepting a more recent low-pressure limit rate constant of Wang et al.[24] k_0(714 K) = 2.21×10^{-27} cm^6

DOI: 10.1021/acs.jpca.5b01276
J. Phys. Chem. A XXXX, XXX, XXX−XXX

molecule^{-2} s^{-1} leads to much higher $x = k_0[M]/k_{inf} = 714$. Using this ratio and the Zhang and Law expressions leads to a smaller deviation of the rate constant at 1 bar from the high-pressure limit of ca. 11%. However, the most recent revisions of the broadening factor in dissociation/recombination reactions by Troe and Ushakov show that the previous expressions overestimated the breadth of the transition region at high $x = k_0[M]/k_{inf}$ values (i.e., very close to the high-pressure limit).[47,48] The predicted deviation of the rate constant from the high-pressure limit at 714 K and 1 bar does not exceed 5%. It should be much smaller at higher pressures taken into account in the averaging (1, 3, 10, and 30 bar). Therefore, we estimate the error associated with the falloff effects at 714 K as not exceeding 2%. On the basis of these estimates, no pressure dependence of the rate constant within the experimental error is expected in accord with the experimental observations.

In view of no pressure dependence observed within the experimental error over the 1−30 bar pressure range and a small drop of the rate constant at 100 bar, we took the average of all measurements over the range 1−30 bar as the high-pressure rate constant of reaction 1. The results are listed in Table 6 and shown in Figure 6. The results were fitted by the expression

$$k_{1,inf} = (5.66 \pm 0.43) \times 10^{-11}(T/298\,K)^{-0.37}$$
$$cm^3\ molecule^{-1}\ s^{-1}\ (292 - 714\,K) \qquad (E8)$$

Table 6. Rate Constant of Reaction 1 ($CH_3 + CH_3 \rightarrow C_2H_6$) in the High-Pressure Limit[a]

temp/K	$k_1/10^{-11}$ cm^3 molecule^{-1} s^{-1}
292	5.61 ± 0.44
354	5.32 ± 0.28
414	5.19 ± 0.42
558	4.39 ± 0.17
626	4.24 ± 0.25
714	4.13 ± 0.19

[a]Experimental data are averaged over the 1−30 bar pressure range. The errors indicated are ±1 std dev.

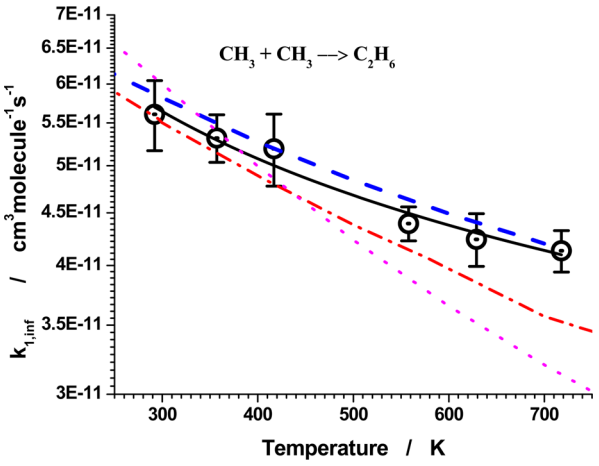

Figure 6. Dotted circles: rate constant k_1 in the high-pressure limit over the temperature range 292−714 K (this work). Error bars: ±1 std dev. Dash-dotted line: Wang et al.[24] Dashed line: Klippenstein et al. (theory).[49] Dotted line: Robertson et al.[50]

Several experimental and theoretical studies are also shown in Figure 5 for comparison (a complete review of the literature could be found in the paper by Blitz et al.[14]). There is excellent agreement at room temperature and a slight difference in the temperature dependence. Current experimental results are in excellent agreement with the theoretical study of Klippenstein et al.[49] over the whole temperature range of this study. At elevated temperatures of this study, the rate constant determined in this work is slightly higher than that obtained by the data extrapolation to the high-pressure limit in the most recent experimental study of Wang et al.[24] (ca. 17% at 714 K).

CONCLUSIONS

Reaction of recombination of methyl radicals was studied over elevated pressure (1−100 bar) and temperature ranges (292−714 K). Currently, at elevated temperatures, these measurements are the closest to the high-pressure limit. A slight drop of the rate constant at 100 bar is reported, and this observation requires further investigation. The rate constant in the high-pressure limit exhibits a negative temperature dependence, in accord with the previous studies. The low-temperature data are in good agreement with the literature, and the results at the elevated temperatures are slightly higher than in the previous measurements, and in excellent agreement with the theoretical calculations of Klippenstein et al.[49]

ASSOCIATED CONTENT

Supporting Information

Complete mechanism used to model the temporal profiles of methyl radicals. The Supporting Information is available free of charge on the ACS Publications website at DOI: 10.1021/acs.jpca.5b01276.

AUTHOR INFORMATION

Corresponding Author

*L. N. Krasnoperov. Fax: (973)-596-8436. E-mail: krasnoperov@adm.njit.edu.

Notes

The authors declare no competing financial interest.

ACKNOWLEDGMENTS

This material is based upon work supported by the National Science Foundation under Grant No. CBET-0827398. We thank Prof. Michael Pilling for sharing the results prior publication.

REFERENCES

(1) Pilling, M. J. Radical-Radical Reactions. *Annu. Rev. Phys. Chem.* **1996**, *47*, 81−108.
(2) Baulch, D. L.; Bowman, C. T.; Cobos, C. J.; Cox, R. A.; Just, T.; Kerr, J. A.; Pilling, M. J.; Stocker, D.; Troe, J.; Tsang, W.; et al. Evaluated Kinetic Data for Combustion Modeling: Supplement II. *J. Phys. Chem. Ref. Data* **2005**, *34*, 757−1397.
(3) Warnatz, J. *Rate Coefficients in the C/H/O System*; Springer-Verlag: New York, 1984; p 197.
(4) Bowman, T.; Hanson, R. K.; Davidson, D. F.; Gardiner, W. C. J.; Lissianski, V.; Smith, G. P.; Golden, D. M.; Frenklach, M.; Goldenberg, M. GRI-Mech 2.11, http://www.me.berkeley.edu/gri_mech/.
(5) Hessler, J. P.; Ogren, P. J. Recombination of Methyl Radicals. 2. Global Fits of the Rate Coefficient. *J. Phys. Chem.* **1996**, *100*, 984−92.
(6) Smith, G. P.; Golden, D. M.; Frenklach, M.; Moriarty, N. W.; Eiteneer, B.; Goldenberg, M.; Bowman, C. T.; Hanson, R.; Song, S.;

DOI: 10.1021/acs.jpca.5b01276
J. Phys. Chem. A XXXX, XXX, XXX−XXX

Gardiner, W. C. J.; et al. GRI-Mech 3.0, http://www.me.berkeley.edu/gri_mech/.
(7) Baulch, D. L.; Cobos, C. J.; Cox, R. A.; Frank, P.; Hayman, G.; Just, T.; Kerr, J. A.; Murrells, T.; Pilling, M. J.; Troe, J.; et al. Evaluated Kinetic Data for Combustion Modeling. Supplement I. *J. Phys. Chem. Ref. Data* **1994**, *23*, 847−848.
(8) Manion, J. A.; Huie, R. E.; Levin, R. D.; Burgess, D. R., Jr.; Orkin, V. L.; Tsang, W.; McGivern, W. S.; Hudgens, J. W.; Knyazev, V. D.; Atkinson, D. B.; et al. NIST Chemical Kinetics Database, NIST Standard Reference Database 17, Version 7.0 (Web Version), Release 1.4.3, Data version 2008.12; National Institute of Standards and Technology: Gaithersburg, MD, 2008; http://kinetics.nist.gov/.
(9) Tsang, W. Chemical Kinetic Data Base for Combustion Chemistry. Part 2. Methanol. *J. Phys. Chem. Ref. Data* **1987**, *16*, 471−508.
(10) Miller, J. A.; Kee, R. J.; Westbrook, C. K. Chemical Kinetics and Combustion Modeling. *Annu. Rev. Phys. Chem.* **1990**, *41*, 345−387.
(11) Westbrook, C. K.; Dryer, F. L. Chemical Kinetics and Modeling of Combustion Processes. *Symp. (Int.) Combust.* **1981**, *18*, 749−767.
(12) Krasnoperov, L. N.; Michael, J. V. High-Temperature Shock Tube Studies Using Multipass Absorption: Rate Constant Results for OH + CH_3, OH + CH_2, and the Dissociation of CH_3OH. *J. Phys. Chem. A* **2004**, *108*, 8317−8323.
(13) Sangwan, M.; Chesnokov, E. N.; Krasnoperov, L. N. Reaction CH_3 + OH Studied over the 294−714 K Temperature and 1−100 bar Pressure Ranges. *J. Phys. Chem. A* **2012**, *116*, 8661−8670.
(14) Blitz, M. A.; N.J.B, G.; Shannona, R. J.; Pilling, M. J.; Seakins, P. W.; Western, C. M.; Robertson, S. H. Reanalysis of Rate Data for the Reaction CH_3+CH_3 → C_2H_6 using Revised Cross-Sections and a Linearised Second Order Master Equation. *J. Phys. Chem. A* **2015**, DOI: 10.1021/acs.jpca.5b01002.
(15) Hippler, H.; Luther, K.; Ravishankara, A. R.; Troe, J. High-Pressure Effects in the Recombination Reaction CH_3 + CH_3 → C_2H_6. *Z. Phys. Chem. Neue Folge* **1984**, *142*, 1−12.
(16) Sangwan, M.; Krasnoperov, L. N. Disproportionation Channel of Self-Reaction of Hydroxyl Radical, OH + OH → H_2O + O, Studied by Time-Resolved Oxygen Atom Trapping. *J. Phys. Chem. A* **2012**, *116*, 11817−11822.
(17) Sangwan, M.; Krasnoperov, L. N. Kinetics of the Gas Phase Reaction CH_3 + HO_2. *J. Phys. Chem. A* **2013**, *117*, 2916−2923.
(18) Sangwan, M.; Chesnokov, E. N.; Krasnoperov, L. N. Reaction CH_3 + OH Studied over the 294 - 714 K Temperature and 1 - 100 bar Pressure Ranges. *J. Phys. Chem. A* **2012**, *116*, 8661−8670.
(19) Sangwan, M.; Chesnokov, E. N.; Krasnoperov, L. N. Reaction OH + OH Studied over the 298−834 K Temperature and 1 - 100 bar Pressure Ranges. *J. Phys. Chem. A* **2012**, *116*, 6282−6294.
(20) Krasnoperov, L. N.; Chesnokov, E. N.; Stark, H.; Ravishankara, A. R. Elementary Reactions of Formyl (HCO) Radical Studied by Laser Photolysis - Transient Absorption Spectroscopy. *Proc. Combust. Inst.* **2004**, *30*, 919−927.
(21) Grebenkin, S. Y.; Krasnoperov, L. N. Kinetics and Thermochemistry of the Hydroxycyclohexadienyl Radical Reaction with O_2: C_6H_6OH + O_2 ⇔ $C_6H_6(OH)O_2$. *J. Phys. Chem. A* **2004**, *108*, 1953−1963.
(22) Lightfoot, P. D.; Kirwan, S. P.; Pilling, M. J. Photolysis of Acetone at 193.3 nm. *J. Phys. Chem.* **1988**, *92*, 4938−4946.
(23) Greenblatt, G. D.; Ravishankara, A. R. Laboratory Studies on the Stratospheric NOx Production Rate. *J. Geophys. Res.* **1990**, *95*, 3539−3547.
(24) Wang, B.; Hou, H.; Yoder, L. M.; Muckerman, J. T.; Fockenberg, C. Experimental and Theoretical Investigations on the Methyl−Methyl Recombination Reaction. *J. Phys. Chem. A* **2003**, *107*, 11414−11426.
(25) Krasnoperov, L. N.; Mehta, K. Kinetic Study of CH_3 + HBr and CH_3 + Br Reactions by Laser Photolysis-Transient Absorption over 1−100 bar Pressure Range. *J. Phys. Chem. A* **1999**, *103*, 8008−8020.
(26) Baklanov, A. V.; Krasnoperov, L. N. Absorption Spectrum and Rate Constant for Self-Reaction of Silyl Radicals. *J. Phys. Chem. A* **2001**, *105*, 4917−4922.
(27) Hahn, J.; Krasnoperov, L.; Luther, K.; Troe, J. Pressure Dependence of the Reaction H + O_2 (+Ar) –> HO_2 (+Ar) in the Range 1−900 bar and 300−700 K. *Phys. Chem. Chem. Phys.* **2004**, *6*, 1997−1999.
(28) Krasnoperov, L. N.; Chesnokov, E. N.; Stark, H.; Ravishankara, A. R. Unimolecular Dissociation of Formyl Radical, HCO –> H + CO, Studied Over 1 - 100 bar Pressure Range. *J. Phys. Chem. A* **2004**, *108*, 11526−11536.
(29) Johnson, D.; Krasnoperov, L. N.; Raoult, S.; Lesclaux, R. UV Absorption Spectra of Methyl-Substituted Hydroxy-Cyclohexadienyl Radicals in the Gas Phase. *J. Photochem. Photobiol., Sect. A: Chem.* **2005**, *176*, 98−106.
(30) Macpherson, M. T.; Pilling, M. J.; Smith, M. J. C. Determination of the Absorption Cross Section for Methyl at 216.36 nm and the Absolute Rate Constant for Methyl Radical Recombination over the Temperature Range 296−577 K. *J. Phys. Chem.* **1985**, *89*, 2268−2274.
(31) Mebel, A. M.; Lin, S.-H. Excited Electronic States of the Methyl Radical. Ab Initio Molecular Orbital Study of Geometries, Excitation Energies and Vibronic Spectra. *Chem. Phys.* **1997**, *215*, 329−341.
(32) Oehlschlaeger, M. A.; Davidson, D. F.; Hanson, R. K. High-temperature UV Absorption of Methyl Radicals Behind Shock Waves. *J. Quant. Spectrosc. Radiat. Transf.* **2005**, *92*, 393−402.
(33) Herzberg, G.; Shoosmith, J. Absorption Spectrum of Free CH_3 and CD_3 Radicals. *Can. J. Phys.* **1956**, *34*, 523−525.
(34) Callear, A. B.; Metcalfe, M. P. Oscillator-Strengths of Bands of $\tilde{B}^2A_1' \leftarrow \tilde{X}^2A_2''$ System of CD_3 and a Spectroscopic Measurement of Recombination Rate - Comparison with CH_3. *Chem. Phys.* **1976**, *14*, 275−284.
(35) *International Thermodynamic Tables of the Fluid State. Helium-4*; Pergamon Press: New York, 1977.
(36) Smoluchowski, M. V. Versuch Einer Mathematischen Theorie der Koagulationskinetic Kolloider Lösunger. *Z. Phys. Chem. Stoechiom. Verwandtschaftsl* **1917**, *92*, 129−168.
(37) Noyes, R. M. A Treatment of Chemical Kinetics with Special Applicability to Diffusion Controlled Reactions. *J. Phys. Chem.* **1954**, *22*, 1349−1359.
(38) Alberty, R. A.; Hammes, G. G. Application of the Theory of Diffusion-Controlled Reactions to Enzyme Kinetics. *J. Phys. Chem.* **1958**, *62*, 154−159.
(39) Franck, J.; Rabinowitch, E. Some Remarks About Free Radicals and the Photochemistry of Solutions. *Trans. Faraday Soc.* **1934**, *30*, 120−131.
(40) Hippler, H.; Otto, B.; Schroeder, J.; Schubert, V.; Troe, J. Diffusion Controlled Atom Recombination and Photolytic Cage Effect of Halogens in Compressed Gases and Liquids. *Ber. Bunsen-Ges. Phys. Chem.* **1985**, *89*, 240−2.
(41) Hippler, H.; Schubert, V.; Troe, J. Photolysis Quantum Yields and Atom Recombination Rates of Bromine in Compressed Gases. Experiments up to 7 kbar. *J. Chem. Phys.* **1984**, *81*, 3931−41.
(42) *CRC Handbook of Chemistry and Physics*, 76th ed.; CRC Press: New York, 1996.
(43) Oum, K.; Luther, K.; Troe, J. High-Pressure Studies of Radical-Solvent Molecule Interactions in the CCl_3 and Bromine Combination Reactions of CCl_3. *J. Phys. Chem. 108*, 2690−2699.
(44) Baulch, D. L.; Cobos, C. J.; Cox, R. A.; Frank, P.; Hayman, G.; Just, T.; Kerr, J. A.; Murrells, T.; Pilling, M. J.; Troe, J.; et al. Evaluated Kinetic Data for Combusion Modelling. Supplement I. *J. Phys. Chem. Ref. Data* **1994**, *23*, 847−1033.
(45) Troe, J. Predictive Possibilities of Unimolecular Rate Theory. *J. Phys. Chem.* **1979**, *83*, 114−126.
(46) Zhang, P.; Law, C.-K. A Fitting Formula for the Falloff Curves of Unimolecular Reactions. *Int. J. Chem. Kinet.* **2009**, *41*, 727−734.
(47) Troe, J.; Ushakov, V. G. Revisiting Falloff Curves of Thermal Unimolecular Reactions. *J. Chem. Phys.* **2011**, *135*, 054304.
(48) Troe, J.; Ushakov, V. G. Representation of "Broad" Falloff Curves for Dissociation and Recombination Reactions. *Z. Phys. Chem.* **2014**, *228*, 1−10.

DOI: 10.1021/acs.jpca.5b01276
J. Phys. Chem. A XXXX, XXX, XXX−XXX

(49) Klippenstein, S. J.; Georgievskii, Y.; Harding, L. B. Predictive Theory for the Combination Kinetics of Two Alkyl Radicals. *Phys. Chem. Chem. Phys.* **2006**, *8*, 1133−1147.
(50) Robertson, S. H.; Pilling, M. J.; Baulch, D. L.; Green, N. J. B. Fitting of Pressure-Dependent Kinetic Rate Data by Master Equation/Inverse Laplace Transform Analysis. *J. Phys. Chem.* **1995**, *99*, 13452−13460.

DOI: 10.1021/acs.jpca.5b01276
J. Phys. Chem. A XXXX, XXX, XXX−XXX